A feasible identification method of uncertainty responses for vehicle structures

Xiang Xu[1], Xinbo Chen[1,2*], Zhe Liu[1], Yong Zhang[3], Yanan Xu[1,4], Jianguang Fang[5], Yunkai Gao[1]

1 School of Automotive Studies, Tongji University, Shanghai 201804, China

2 Clean Energy Automotive Engineering Center, Tongji University, Shanghai 201804, China

3 College of Mechanical Engineering and Automation, Huaqiao University, Xiamen 361021, China

4 School of Aerospace, Mechanical and Mechatronic Engineering, The University of Sydney, NSW 2006, Australia

5 School of Civil and Environmental Engineering, University of Technology Sydney, Sydney, NSW, 2007, Australia

Abstract:

Many unavoidable uncertainties in the engineering structure will affect its performance response. It is necessary to analyze the uncertain responses generated by uncertain factors in the vehicle design. Therefore, this study proposes a feasible identification method of uncertainty responses for vehicle structures. The proposed method consists of radial basis function neural network (RBFNN) and Taylor interval expansion (IE) model. The optimal network parameters of RBFNN are trained by the improved K-means clustering algorithm and singular value decomposition (SVD). Here, the first-order and second-order differential equations are derived from the RBFNN parameters since it is difficult to calculate the partial derivatives of complex systems without explicit expressions. A series of typical functions are tested and the results show that the trained RBFNN parameters can approximate the first-order and second-order partial derivatives of different types of functions. Besides, the subinterval expansion method is further applied to improve the calculation accuracy of uncertain structural responses. Finally, the proposed method is applied to four engineering applications (vehicle hood, mechanical claw, anti-collision structures, and multi-link suspension). Compared with genetic algorithm (GA) and Monte Carlo simulation (MCS), the proposed method can improve computational efficiency while ensuring accuracy. The identification method of interval uncertainty responses can be used as an alternative for uncertainty analysis and subsequent reliability or robustness optimization.

Keywords: Vehicle structure analysis; Uncertain problem; Interval model; Radial basis function.

* Corresponding author.

E-mail address: xiangxu_93@163.com (X. Xu), austin_1@163.com (X. Chen).

1. Introduction

Uncertainty of design parameters often arises in structural design, and even slight uncertainty may produce large fluctuations in the output response (Cao et al. 2021; Meng et al. 2020; Chen and Yang 2021; Long et al. 2019; Xu et al. 2021a). The influence of uncertain parameters is an essential topic in engineering design. Researchers considered uncertain parameters and system responses as probability values in the early days (Huang et al. 2016; Xu et al. 2021b; Gao et al. 2018). Inevitably, a probabilistic uncertain model needs a large number of statistical samples, which may be challenging due to the lack of test conditions. In this regard, the unknown-but-bounded model gradually attracts the attention of researchers (Xia et al. 2015; Wu et al. 2014; Wang et al. 2020). Because the interval model only needs to consider the interval boundary problem and no longer needs statistical data, it has higher practicability than the probability model (Tang et al. 2021; Viegas et al. 2017; Ma and Wang 2021; Qiu and Li 2021).

Over the past decade, strategies for solving the lower and upper bounds of interval models are gradually proposed (Chen et al. 2009; Impollonia and Muscolino 2011). When the interval model is regarded as a bounded uniform distribution model, Monte Carlo simulation (MCS) can solve the interval model. The lower and upper bounds of responses can be predicted by random sampling technique (Gao et al. 2011; Qiu and Wang 2005b; Guo, et al. 2008). By increasing the number of samples, MCS can gradually converge to an exact interval. However, MCS is unsuitable for practical engineering problems because of the expensive computational cost, so more efficient alternative methods should be studied. Besides, the auxiliary global optimization algorithm is introduced to solve the interval model. Li et al. proposed an adaptive Kriging method for structures with uncertain-but-bounded parameters and used sequential quadratic programming (SQP) as the inner solver to obtain the lower and upper bounds (Li et al. 2013). The genetic algorithm (GA), which provides practical search ability in a complex space based on natural genetics, is feasible to calculate the interval bounds of the objective function and constraint function of internal optimization (Fernandez-Prieto et al. 2012). Jiang et al. used the intergeneration projection genetic algorithm (IP-GA) as an optimization operator to search for the lower and upper bounds (Jiang et al. 2008a; Jiang et al. 2008b). Cheng et al. proposed a direct interval optimization algorithm for the reliability model integrating GA and Kriging technology (Cheng et al. 2016). This method avoids the complex transformation of the indirect model

and gives an interval solution. The most significant advantage of the intelligent algorithm is the ability to find the global optimum, but its optimization often requires a large amount of calculation, especially for some complex engineering problems. Another alternative method is the interval vertex method (IVM), aiming at solving linear interval equations. It can obtain a more accurate value with higher efficiency than the intelligent algorithm. Qiu et al. (Qiu et al. 2006; Qiu et al. 2007) gave a mathematical proof of the vertex solution theorem and applied it to calculate structural design with unknown-but-bounded parameters. Unfortunately, the application of IVM is limited to monotone cases and is unsuitable for complex nonlinear problems.

In addition, the approximate method of Taylor expansion has also interested researchers because it can produce approximate solutions close to the exact solutions. Qiu et al. (Qiu et al. 1996; Qiu and Wang 2005a) proposed an interval perturbation method by using the Taylor series to expand the interval matrix and interval vector. Generally, due to the complexity of the higher-order Taylor series, only the terms of first-order or second-order Taylor series were retained in the commonly used interval perturbation. Wu et al. (Wu et al. 2005) used the first-order Taylor expansion method to analyze the dynamic response of linear structural systems with interval parameters. Zhang et al. (Zhang et al. 2007) used the matrix perturbation theory and the interval algorithm to estimate the lower and upper bounds of the dynamic response of a closed-loop system with interval parameters. Qiu et al. (Qiu et al. 2009) studied the dynamic responses of uncertain nonlinear vibration systems and estimated the range of nonlinear dynamic responses based on the second-order Taylor series expansion method by using the mathematical interval method. However, the interval expansion method of Taylor approximation needs the partial derivative information of the model. In a nonlinear system without expression, the partial derivative information can be hardly obtained directly by using the conventional auxiliary calculation method, which hinders the application of Taylor approximation expression in the interval model.

In recent years, the modeling methods of machine learning in system response approximation have gradually been developed (Rageh et al. 2020; Imani et al. 2021). The artificial neural network is a kind of machine learning, which has a good research prospect in the field of engineering (Sharifzadeh et al. 2019). It is found that the generalized radial basis function neural network (RBFNN) has an advantage in approximating system functions and solving partial derivatives (Almarashi 2012). Chen et al. (Chen et al. 2011) proposed a method combining a radial basis function network and an adaptive

residual sub-sampling training scheme to solve the partial differential equation. Brown et al. (Brown et al. 2005) employed the approximate cardinal function preprocessing technique to solve the partial differential equations of radial basis functions. The RBFNN with self-defined preset features is highly accurate in solving partial derivative problems and thus can be regarded as an alternative method to obtain partial derivatives.

Therefore, considering the low computational cost of Taylor expansion, this study uses the RBFNN as an auxiliary to solve the differential equations, which can improve the applicability of the Taylor expansion in the interval models. Simultaneously, to improve the efficiency and accuracy of the interval expansion, this study set up the method of dimension reduction of multivariate uncertain parameters and subinterval model. Section 2 gives the basic interval model theory. Section 3 presents the derivation of partial differential equations and typical function testing. Section 4 analyzes the four engineering examples. The main conclusions are drawn in Section 5.

2. Interval model theory

2.1 Interval uncertainty model

The unknown-but-bounded uncertain parameters can be represented by the interval model. For the interval value x,

$$x = [x^{IL}, x^{IU}] = \{I | x^{IL} \le I \le x^{IU}, I \in R\} \tag{1}$$

where x^{IL} and x^{IU} are the lower and upper bounds of x, respectively. I is a possible value of x, and R is a set of real numbers. Here, if the nominal value of x is regarded as the median value, the interval radius of x is the deviation range. Interval radius x^{IR} and median value x^{IM} are

$$x^{IR} = \frac{x^{IU} - x^{IL}}{2}, \qquad x^{IM} = \frac{x^{IU} + x^{IL}}{2} \tag{2}$$

If $x^{IR} = 0$, x degenerates to a definite real number. The basic operation method between two interval values (x_1, x_2) is defined as follows:

$$x_1 + x_2 = [x_1^{IL} + x_2^{IL}, x_1^{IU} + x_2^{IU}] \tag{3}$$

$$x_1 - x_2 = [x_1^{IL} - x_2^{IU}, x_1^{IU} - x_2^{IL}] \tag{4}$$

$$x_1 \times x_2 = [\min(x_1^{IL}x_2^{IL}, x_1^{IL}x_2^{IU}, x_1^{IU}x_2^{IL}, x_1^{IU}x_2^{IU}), \max(x_1^{IL}x_2^{IL}, x_1^{IL}x_2^{IU}, x_1^{IU}x_2^{IL}, x_1^{IU}x_2^{IU})] \tag{5}$$

$$\frac{x_1}{x_2} = x_1 \times \left(\frac{1}{x_2}\right), \qquad \left(\frac{1}{x_2}\right) = \begin{cases} \emptyset, \ \ x_2 = [0,0] \\ [1/x_2^{IU}, 1/x_2^{IL}], \quad 0 \notin x_2 \\ [1/x_2^{IU}, \infty], \quad x_2^{IL} = 0, x_2^{IU} = 0 \\ [-\infty, 1/x_2^{IL}], \quad x_2^{IL} < 0, x_2^{IU} = 0 \\ [-\infty, \infty], \quad x_2^{IL} < 0, x_2^{IU} > 0 \end{cases} \tag{6}$$

It is efficient for some simple continuous functions to use the above operation method.

2.2 Taylor interval expansion model

Taylor expansion can approximately express some complex functions as simple polynomials. Taylor expansion at the point $\mathbf{x}^{IM}$ is

$$f(\mathbf{x}) = f(\mathbf{x}^{IM}) + (\nabla \mathbf{f})^T(\mathbf{x} - \mathbf{x}^{IM}) + \frac{1}{2}(\mathbf{x} - \mathbf{x}^{IM})^T \mathbf{H}(\mathbf{x} - \mathbf{x}^{IM}) + O^{n_t} \tag{7}$$

where O^n is the n_t order Taylor remainder and $\mathbf{H}$ is Hessian matrix. For m-dimensional $\mathbf{x}$,

$$\mathbf{H} = \begin{bmatrix} \frac{\partial^2 f(x_1^{IM})}{\partial x_1^2} & \frac{\partial^2 f(x_2^{IM})}{\partial x_1 \partial x_2} & \cdots & \frac{\partial^2 f(x_m^{IM})}{\partial x_1 \partial x_m} \\ \frac{\partial^2 f(x_2^{IM})}{\partial x_2 \partial x_1} & \frac{\partial^2 f(x_2^{IM})}{\partial x_2^2} & \cdots & \frac{\partial^2 f(x_m^{IM})}{\partial x_2 \partial x_m} \\ \vdots & \vdots & \ddots & \vdots \\ \frac{\partial^2 f(x_m^{IM})}{\partial x_m \partial x_1} & \frac{\partial^2 f(x_m^{IM})}{\partial x_m \partial x_2} & \cdots & \frac{\partial^2 f(x_m^{IM})}{\partial x_m^2} \end{bmatrix} \tag{8}$$

To improve the computational efficiency, only the second-order expansion and the data on the diagonal of the Hessian matrix are retained in this study, as shown Eq. (9).

$$\widetilde{\mathbf{H}} = \begin{bmatrix} \frac{\partial^2 f(x_1^{IM})}{\partial x_1^2} & 0 & \cdots & 0 \\ 0 & \frac{\partial^2 f(x_2^{IM})}{\partial x_2^2} & \cdots & 0 \\ \vdots & \vdots & \ddots & \vdots \\ 0 & 0 & \cdots & \frac{\partial^2 f(x_m^{IM})}{\partial x_m^2} \end{bmatrix} \tag{9}$$

Besides, the dimension reduction of multivariate uncertain parameters can be carried out, the Taylor expansion can be divide into different Taylor expansions that only has one uncertain parameter, as shown Eq. (10) to Eq. (11).

$$f(\mathbf{x}) \approx \tilde{f}(\mathbf{x}) = f_1(x_1, x_2^{IM}, x_3^{IM} \ldots x_m^{IM}) + \cdots + f_m(x_1^{IM}, x_2^{IM}, x_3^{IM} \ldots x_m) - (m-1) f(\mathbf{x}^{IM}) \tag{10}$$

$$f_k \approx f_k(x_k^{IM}) + \frac{\partial f_k(x_k^{IM})}{\partial x_k}(x_k - x_k^{IM}) + \frac{1}{2}\frac{\partial^2 f_k(x_k^{IM})}{\partial {x_k}^2}(x_k - x_k^{IM})^2, k = 1,2,\dots,m \tag{11}$$

Therefore, the lower and upper bounds of f_k and $f(\mathbf{x})$ can be expressed as

$${f_k}^{IL} = f_k(x_k^{IM}) - \left|\frac{\partial f_k(x_k^{IM})}{\partial x_k}\right|(x_k^{IR}) - \left|\frac{1}{2}\frac{\partial^2 f_k(x_k^{IM})}{\partial {x_k}^2}\right|(x_k^{IR})^2 \tag{12}$$

$${f_k}^{IU} = f_k(x_k^{IM}) + \left|\frac{\partial f_k(x_k^{IM})}{\partial x_k}\right|(x_k^{IR}) + \left|\frac{1}{2}\frac{\partial^2 f_k(x_k^{IM})}{\partial {x_k}^2}\right|(x_k^{IR})^2 \tag{13}$$

$$f(\mathbf{x}) = \left[\left(\sum_{k=1}^{m} {f_k}^{IL} - (m-1)f(\mathbf{x}^{IM})\right), \left(\sum_{k=1}^{m} {f_k}^{IU} - (m-1)f(\mathbf{x}^{IM})\right)\right] \tag{14}$$

Then, the Taylor interval expansion (IE) model can be expressed by Eq. (14). Generally, the Taylor formula can achieve the best approximation in the case of very small interval radius (x_k^{IR}). Therefore, the calculation accuracy can be improved by establishing subintervals to compensate for the approximation error. For the uncertainty parameters $\mathbf{x}$,

$$\mathbf{x}_{s\_i} = \left[\mathbf{x}^{IL} + \frac{2(s\_i - 1)\mathbf{x}^{IR}}{S\_n}, \mathbf{x}^{IL} + \frac{2s\_i\mathbf{x}^{IR}}{S\_n}\right], s\_i = 1,2,\dots,S\_n. \tag{15}$$

where $\mathbf{x}_{s\_i}$ and S_n are the s_i th subinterval and the subinterval number, respectively. The subinterval number can be determined by referring to the number of uncertain parameters.

3. Interval expansion method

3.1 Radial basis function neural network

RBFNN, which has the characteristics of self-learning, self-adaptive, and fast learning speed (Warnes et al. 1998; Leonard et al. 1992; Zhang et al. 2020), is chosen as the approximate model of the original system in this study. RBFNN is a simple three-layer neural network, including an input layer, a hidden layer, and an output layer, as shown in **Fig. 1.** Gaussian functions are often used as radial basis functions as follows:

$$r_j(\|\mathbf{x} - \mathbf{c}_j\|) = \exp\left(-\frac{1}{2\delta_j^2}\|\mathbf{x} - \mathbf{c}_j\|^2\right), \quad j = 1,2,\dots,n \tag{16}$$

where $\mathbf{x}$ is the input, $\mathbf{c}_j$ is the center of j^{th} basis functions, and δ_j^2 is the variance of the radial basis

function. $\|.\|$ is the Euclidian distance and n is the number of nerurons. For one output $f(\mathbf{x})$, the final output of the neural network can be expressed as:

$$f(\mathbf{x}) = \sum_{j=1}^{n} \omega_j r_j(\|\mathbf{x} - \mathbf{c}_j\|) + \omega_0, \quad j = 1,2,\dots,n \tag{17}$$

where ω_j is the weight from the hidden layer to the output layer.

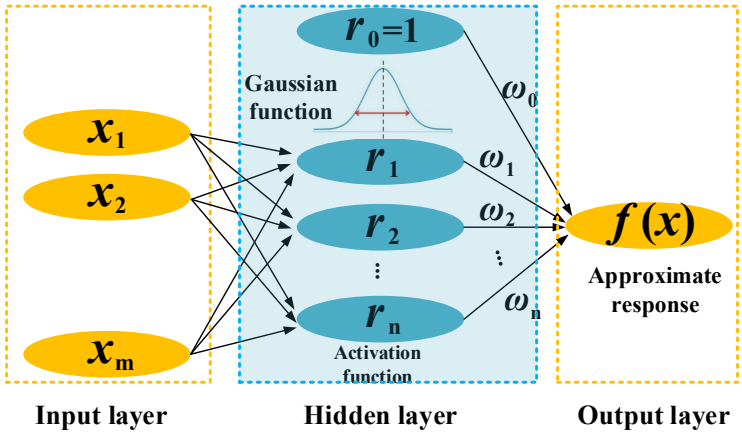

Fig. 1 RBFNN with Gaussian function.

To obtain a high-precision approximate model, the main network parameters of RBFNN (center point c, variance δ^2 and weight ω) need to be determined. Let the input dimension be m, and the number of training samples be P $(P > m)$. The hidden layer is aimed to map the input from low dimension m to high dimension P, which transforms a linear non-separable low-dimensional linear case into a linear separable high-dimensional case. When the number of neurons is equal to the number of samples, meanly $P = n$, the center of each neuron is the value of each sample. Inevitably, the above methods are time-consuming. Therefore, the number of neurons is usually less than the number of samples ($P > n$). Here, P samples are allocated into n clusters, center of which in Euclidean space can be regarded as the center of the radial basis function. K-means clustering algorithm is often used to determine the center position in the input samples (Awad and Qasrawi 2018), but general K-means clustering algorithm is highly dependent on the initial center. Therefore, the improved K-means algorithm is used to design the clusters. The main steps are as follows:

Step 1: Determine the number of cluster centers n, and select the first cluster center $\mathbf{c}_j(0)$ from the dataset randomly;

Step 2: Calculate the distance $D(\mathbf{x}_i)$ between each sample in the dataset and the nearest cluster center

Step 3: Select the next cluster center according to a roulette method, and select probability of each sample as the next cluster center $D(\mathbf{x}_i)^2/\mathrm{sum}(D(\mathbf{x}_i)^2)$;

Step 4: Repeat steps 2 and 3, and set the initial cluster centers as $\mathbf{c}_j(0), j = 1,2,\dots,n$;

Step 5: Classify $\mathbf{x}_i$ into the cluster $j(\mathbf{x}_i)$ center by the nearest distance

$$j(\mathbf{x}_i) = \arg\min_j \left\|\mathbf{x}_i - \mathbf{c}_j(k)\right\| \tag{18}$$

where the k is the number of iterations.

Step 6: Update the cluster center by Eq. (20):

$$\mathbf{c}_j(k) = \frac{\sum_1^{n_j} \mathbf{x}_i}{n_j} \tag{19}$$

where n_j is the number of data points in j^{th} cluster;

Step 7: Recalculate the distance between each data point and the new clustering center. When the clustering center no longer changes, it means the clustering algorithm is convergent. Otherwise, repeat the above steps.

After determining the standard deviation, δ_j^2 can be calculated directly.

$$\delta_1^2 = \delta_2^2 = \delta_j^2 = \cdots = \delta_n^2 = \frac{{d_{\max}}^2}{2n} \tag{20}$$

where $d_{\max}$ is the maximum distance between the cluster centers. Here, singular value decomposition (SVD) is applied to optimize the weights. For an $M \times N$ activation matrix $\mathbf{A}$, the SVD for $\mathbf{A}$ is

$$[\mathbf{U}, \mathbf{S}, \mathbf{V}] = \mathrm{svd}(\mathbf{A}) \tag{21}$$

$$\mathbf{S} = \mathrm{diag}(a_1, a_2, \dots) \tag{22}$$

$\mathbf{U}$ is an $M \times M$ matrix, $\mathbf{V}$ is an $N \times N$ matrix, and $\mathbf{S}$ is an $M \times N$ diagonal matrix. The value on the main diagonal of $\mathbf{S}$ is the singular value of $\mathbf{A}$.

$$\mathbf{A} = \mathbf{USV^T} \tag{23}$$

$$\mathbf{A^+} = \mathbf{U}\mathrm{diag}\left(\frac{1}{a_1}, \frac{1}{a_2}, \dots\right)\mathbf{V^T} \tag{24}$$

For the input and output relations in RBFNN, the expected output of RBFNN, $\mathbf{O}$, is:

$$\mathbf{O} = \mathbf{R}\boldsymbol{\omega} \tag{25}$$

where $\boldsymbol{\omega}$ is the weight vector and $\mathbf{R}$ is the matrix to be singular decomposed, which is composed of a radial basis function matrix and an identity matrix. Then, $\boldsymbol{\omega}$ is calculated by Eq. (26)

$$\boldsymbol{\omega} = \mathbf{R^+O} = [\mathbf{U}\mathrm{diag}\left(\frac{1}{a}\right)\mathbf{V^T}]\mathbf{O} \tag{26}$$

The relative average absolute error ($RAAE$) is presented as the condition to judge whether RBFNN converges or the number of neuron should be increased.

$$RAAE = (1/P_{test}) \frac{\sum_{v=1}^{P_{test}} |O_v - \widetilde{O_v}|}{|O_v|} \leq \varepsilon \tag{27}$$

where P_{test} is the number of test samples and ε is the accuracy requirement, O_v and $\widetilde{O_v}$ are expected output and actual output respectively. The detailed training flowchart is shown in **Fig. 2**. In each iteration, when $RAAE$ is larger than ε, one neuron will be added in turn until the accuracy satisfies the convergence condition. The total samples are obtained by using optimized Latin hypercube sampling (OLHS). If the accuracy $\varepsilon = 0.001$ still does not meet the requirements, the training samples need to be increased when the maximum number of cluster centers is equal to the number of training samples. Finally, the trained network parameters will be saved for further research.

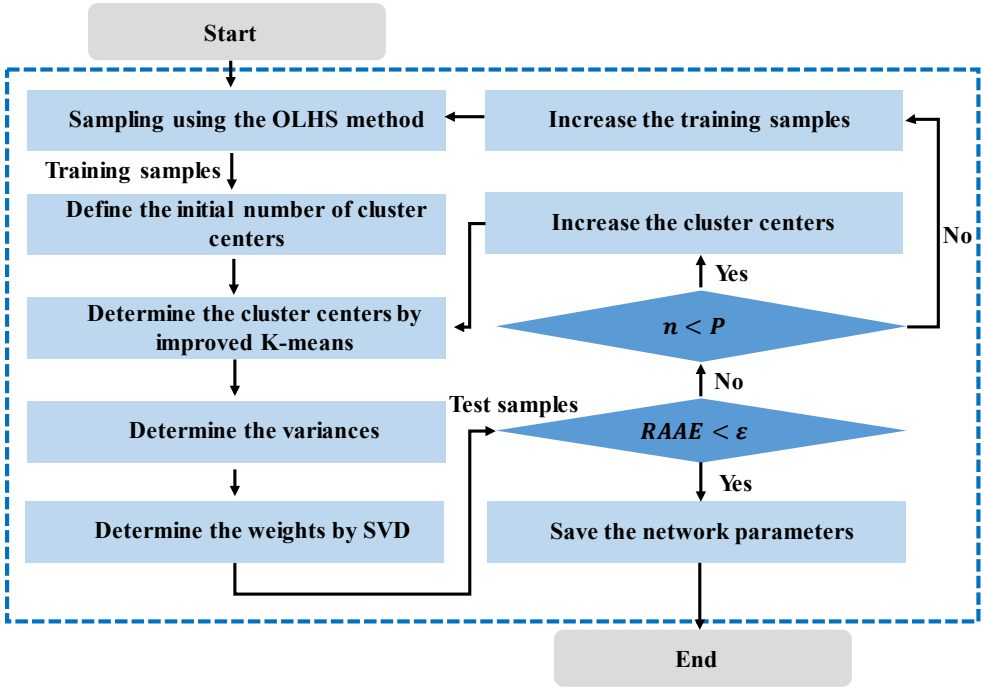

Fig. 2 Training framework of RBFNN.

3.2 Differential equations

The trained approximation model can be used to express the differential equation of the system model. For the input variable x_i, the derivatives of the function are calculated by

$$\frac{\partial f}{\partial x_i} = \sum_{j=1}^{n} -\frac{1}{\delta_j^2} \omega_j \, r_j(\|\mathbf{x} - \mathbf{c}_j\|)(x_i - c_{ji}) \tag{28}$$

$$\frac{\partial^2 f}{\partial x_i^2} = \sum_{j=1}^{n} -\frac{1}{\delta_j^2}\omega_j\, r_j\left(\|\mathbf{x}-\mathbf{c}_j\|\right)\left[1-\frac{1}{\delta_j^2}\left(x_i-c_{ji}\right)^2\right] \tag{29}$$

Without losing generality, the second partial derivatives of different variables $(x_i,\ x_{i+1})$ can be expressed as

$$\frac{\partial^2 f}{\partial x_i x_{i+1}} = \sum_{j=1}^{n} \frac{1}{\delta_j^4}\omega_j\, r_j\left(\|\mathbf{x}-\mathbf{c}_j\|\right)\left(x_i-c_{ji}\right)\left(x_{i+1}-c_{j(i+1)}\right) \tag{30}$$

To explore the feasibility of RBFNN in solving continuous partial derivatives, 6 simple functions are used for verification. These test functions include linear and nonlinear functions, multivariate polynomials, and trigonometric functions.

$$\begin{cases} f_1 = 2x_1 + x_2 + 4x_3 + 3x_4 \\ f_2 = 2x_1x_2 + 5x_2x_3 + 3x_1x_3 + 2x_3x_4 \\ f_3 = \sin(x_1) + 2\sin(x_2) + 3\cos(x_3) + \sin(2x_4) \\ f_4 = 2x_1^2 + x_2^2 + 3x_3^2 + x_4^2 + x_1x_3 + x_2x_3 \\ f_5 = 2x_1^3 + x_2^3 + 3x_3^3 + x_4^3 + x_1x_3 + x_2x_3 \\ f_6 = \sin(x_1) + 2\cos(x_2) + 3\sin(x_4) + x_1x_2x_3x_4 \\ \quad x_1, x_2, x_3, x_4 \in [1,3] \end{cases} \tag{31}$$

Each test function uses 90 samples as training data, and the other 9 samples as testing. The first-order and second-order derivatives of the output values with respect to the input values are calculated. As illustrated in **Fig. 3** and **Fig. 4**, all the test samples are well attached to the partial derivative curve. The network parameters obtained by RBFNN can effectively reflect the derivative trend of the original function.

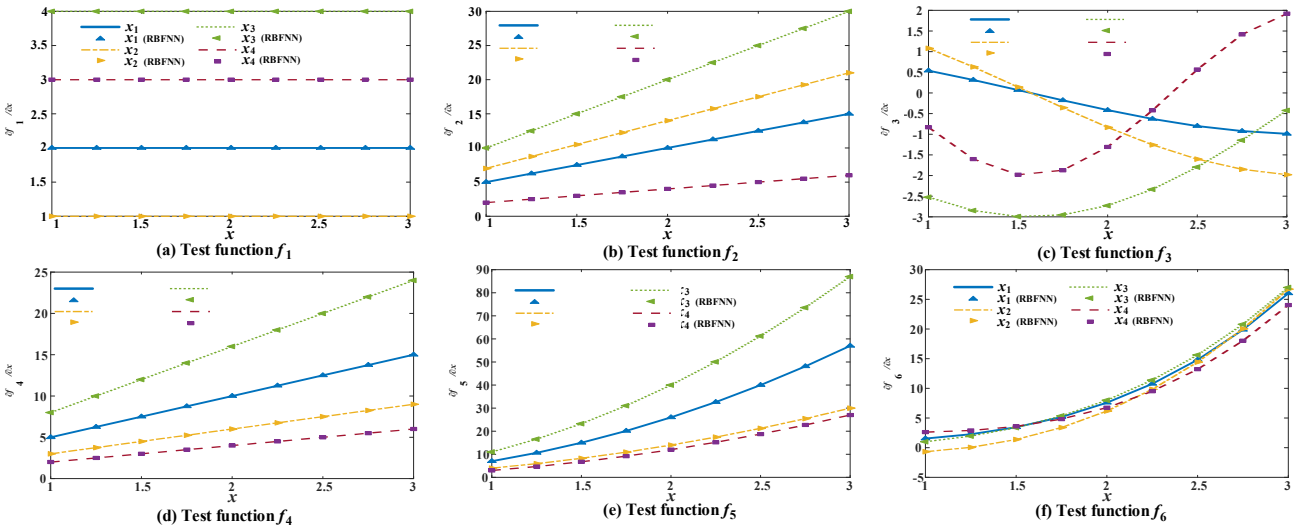

Fig. 3 The first-order differential values of test function.

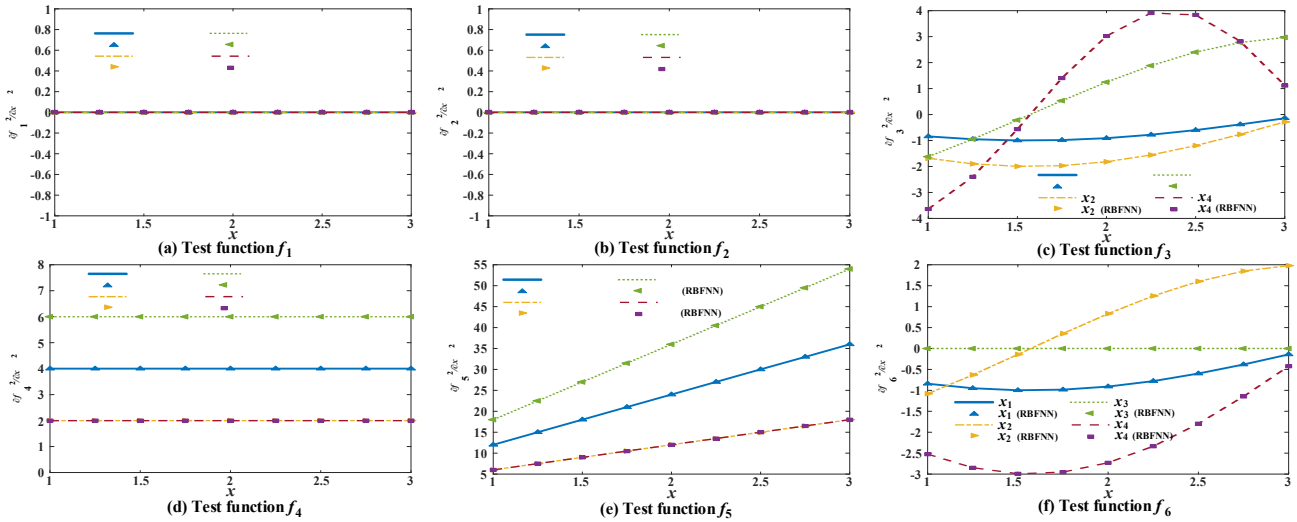

Fig. 4 The second-order differential values of test function.

Here, the $RAAE$s of test samples are shown in **Table 1**. Although the accuracy of the original approximation model is high (maximum error is 0.0006), the relative error of RBFNN rises with the increase of derivative order (the maximum error of the second-order derivatives is 0.0181). Overall, the derivative information of RBFNN has a high fitting capacity for continuous linear and nonlinear functions. In this study, the neural network using Gaussian function as radial basis function is acceptable for solving derivatives of general functions.

Table 1. Relative average errors of the differential functions.

Test functions	Approximate function	First-order	Second-order
f_1	0.0000	0.0005	0.0008
f_2	0.0000	0.0007	0.0008
f_3	0.0006	0.0069	0.0121
f_4	0.0004	0.0042	0.0087
f_5	0.0004	0.0044	0.0107
f_6	0.0006	0.0076	0.0181

3.3 Identification method of uncertainty responses

Obtaining derivative information of complex expressionless structural responses in the Taylor expansion model is difficult. To solve the limitations of the existing interval analysis methods, the RBFNN, and their differentiations are designed into the Taylor expansion model. A novel feasible identification method (RBFNNIE) of uncertainty responses using RBFNN and Taylor IE is proposed. Here, RBFNN can replace the original model to obtain the first-order and second-order partial derivatives. The flowchart of the solving process is shown in **Fig. 5**, which can be described as follows. Firstly, the uncertain parameters are determined, and the training data are prepared for the neural network. Then, the optimal neural network parameters are obtained by a clustering algorithm and singular value decomposition. After that, the first and second partial derivatives of the response model are obtained from the neural network which meets the accuracy requirements. Finally, the lower and upper bounds of responses are constructed by using RBFNNIE.

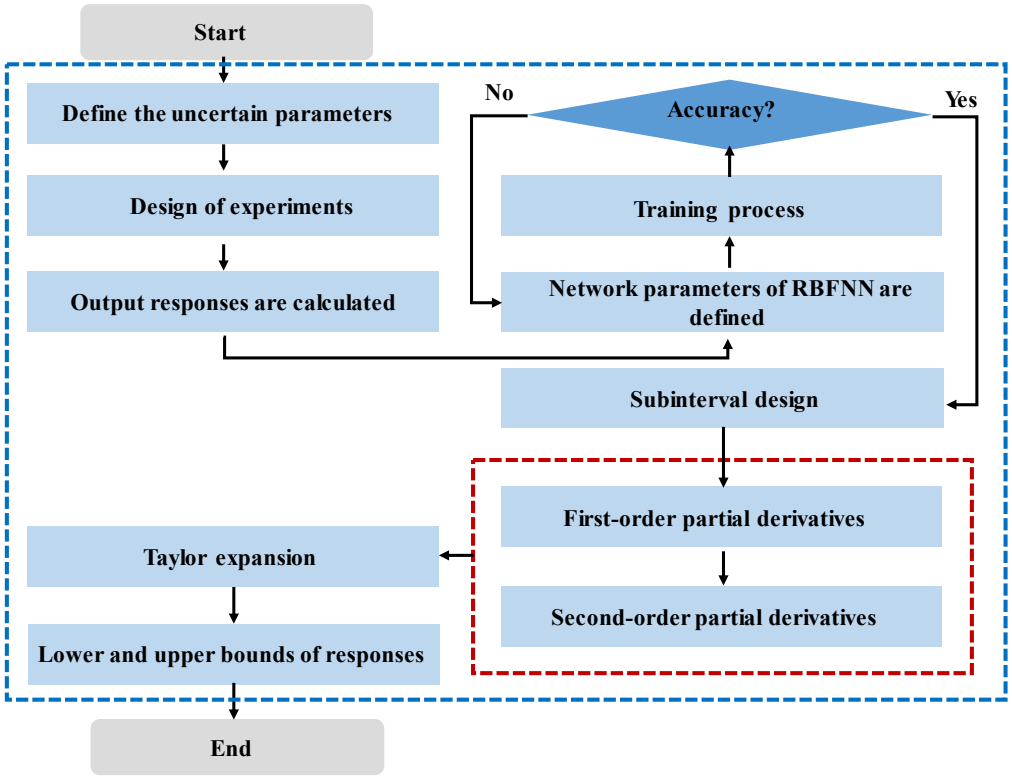

Fig. 5 Flow chat of interval bounds analysis.

4. Interval uncertainty analysis of vehicle structures

4.1 Vehicle hood

Vibration characteristic is an essential index in the design of a vehicle hood. In this section, the 2010 Toyota Yaris (2016) finite element model is adopted to establish the modal analysis model of the vehicle hood. In **Fig. 6** (b), the vehicle hood mainly consists of an inner panel and an outer panel. The nominal thicknesses of the inner and outer panels are 0.5 mm and 0.7 mm respectively. When the uncertainty of thickness parameters is not considered, the first natural frequency of the vehicle hood is 27.13Hz (**Fig. 6** (c)). The two thicknesses of the inner and outer panels are regarded as interval uncertainty parameters, and seven cases are analyzed in which the uncertainty level coefficient ξ of interval parameters are ±0.05, ±0.075, ±0.1, ±0.125, ±0.15, ±0.175, and ±0.2, respectively. Here, the interval uncertainty level coefficient ξ of the design parameter is given to represent different uncertainty ranges.

$$\xi = \left| \frac{x_i^{IR}}{x_i^{IM}} \right| \tag{32}$$

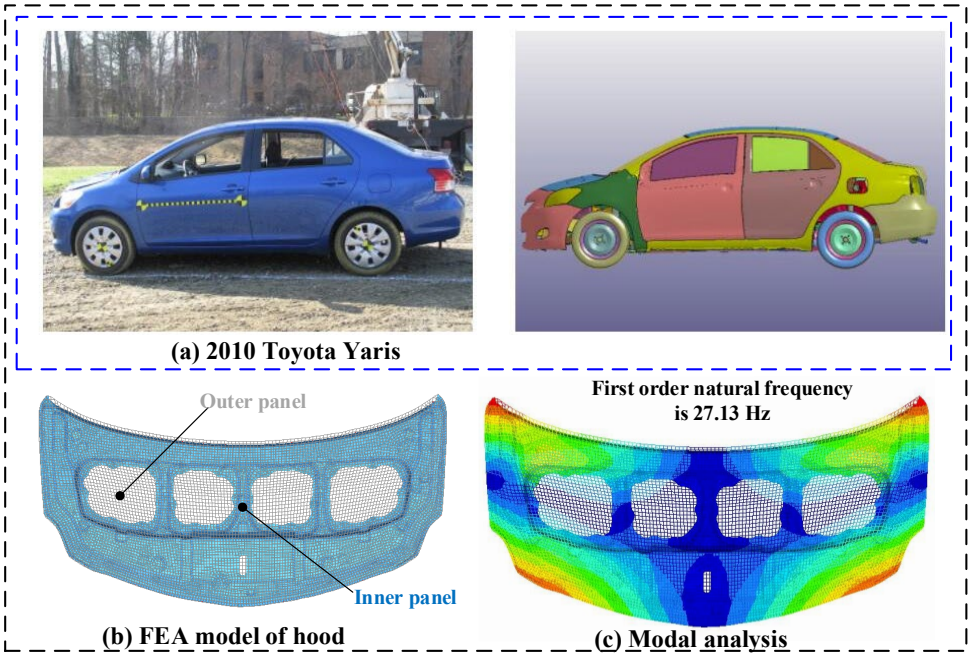

Fig. 6 Vehicle hood from 2010 Toyota Yaris (2016).

Due to the good global convergence of genetic algorithm (GA), the boundary extremum of structural response function can be accurately obtained by setting reasonable algorithm parameters. Therefore, this study uses a genetic algorithm to obtain the boundary values as the accurate values. In

addition, Monte Carlo simulation (MCS) is also used to solve the response bounds as an existing method. Four subintervals are implemented in the uncertainty space. The GA solver comes from MATLAB 2020b. The computer is configured with Inter(R) Core(TM) I5–8250 U CPU@1.6 GHz.

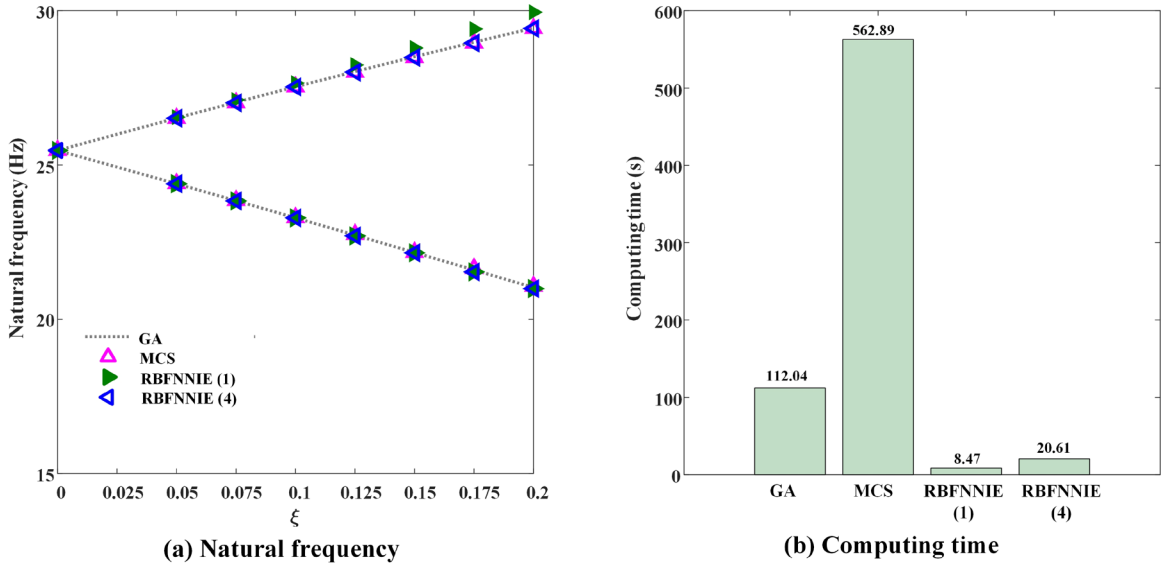

(a) Natural frequency **(b) Computing time**

Fig. 7 Uncertainty analysis of vehicle hood.

Table 2 Relative absolute errors of vehicle hood with different analysis methods

ξ	Lower bound			Upper bound		
	MCS	RBFNNIE (1)	RBFNNIE (4)	MCS	RBFNNIE (1)	RBFNNIE (4)
0.05	0.0004	0.0001	0.0000	0.0002	0.0011	0.0002
0.075	0.0003	0.0003	0.0003	0.0007	0.0028	0.0007
0.100	0.0004	0.0000	0.0001	0.0002	0.0044	0.0008
0.125	0.0005	0.0011	0.0002	0.0007	0.0076	0.0019
0.150	0.0003	0.0005	0.0003	0.0008	0.0098	0.0054
0.175	0.0023	0.0029	0.0014	0.0010	0.0148	0.0065
0.200	0.0020	0.0017	0.0016	0.0005	0.0174	0.0091

As shown in **Fig. 7**, the results of different uncertainty interval bounds are presented. RBFNNIE (1) and RBFNNIE (4) represent the expansion methods of one interval and four subintervals respectively. Compared with GA, MCS and RBFNNIE can effectively approximate the lower and upper bounds of the natural frequency. However, GA and MCS need to consume a lot of calculation

time in the actual calculation process. As shown in **Fig. 7** (b), the average calculation time of GA and MCS is 112.04s and 562.89s respectively, while RBFNNIE (1) and RBFNNIE (4) only need 8.47 and 20.61s respectively. It indicates that RBFNNIE has higher efficiency. On the other hand, the relative absolute errors of MCS and RBFNNIE to GA are given in **Table 2**. The maximum error of MCS appears in the lower bound with $\xi = 0.175$, and the maximum error of RBFNNIE occurs in the upper bound with $\xi = 0.2$. Moreover, RBFNNIE (4) has higher accuracy than RBFNNIE (1). RBFNNIE (4) can achieve a similar accuracy of MCS and requires lower computational cost. It shows that RBFNNIE has a good approximation ability for the lower and upper bounds, and can improve the accuracy by adding subintervals. The proposed method can be used to analyze the vibration mode problem.

4.2 Mechanical claw

To promote the development of intelligent sanitation vehicles, automatic mechanical claws are designed in this work. As shown in **Fig. 8** (a), the preliminary drawing is established in SolidWorks. In the work process, the left and right mechanical claws are used to grab trash cans. The mechanical claw mainly bears the horizontal extrusion reaction force and the vertical friction force. The horizontal force F_2 and the vertical force F_1 are 1466N and 910N, respectively.

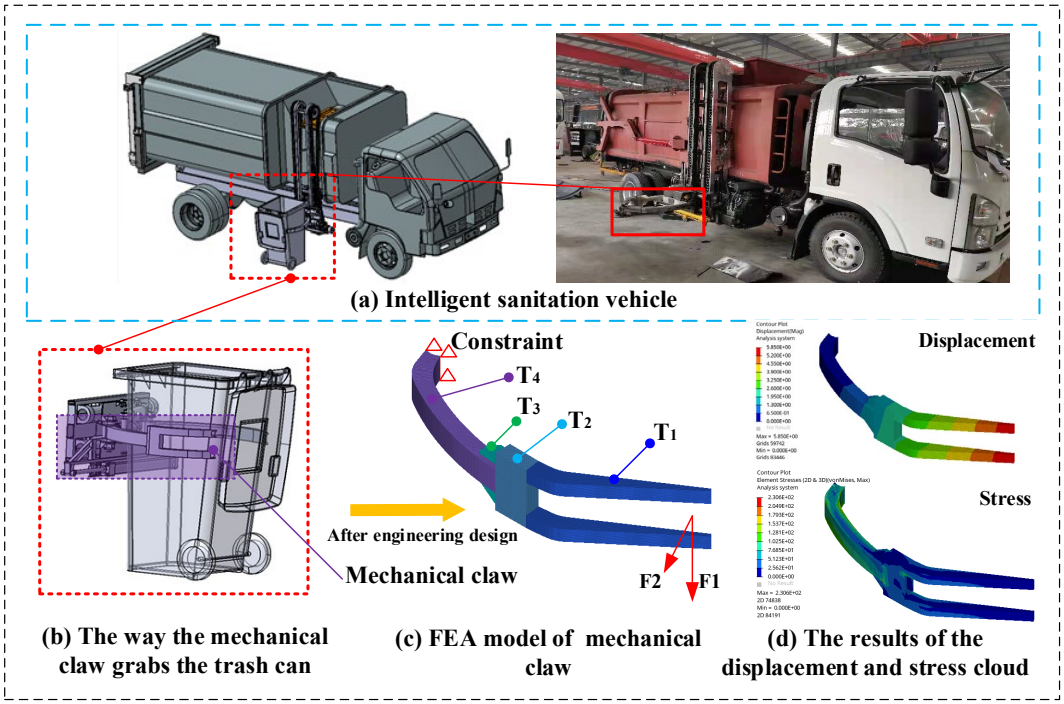

Fig. 8 Loading analysis of mechanical claw.

The FEA model of the mechanical claw is established by OptiStruct (as presented in **Fig. 8** (c)).

The mechanical claw mainly includes four thickness variables (T_1, T_2 T_3 and T_4 are 5mm), and the material is No.45 steel. To investigate the loading characteristics of the mechanical claw, the finite element analysis is conducted and the results are shown in **Fig. 8** (d). T_1, T_2 T_3 and T_4 are regarded as interval uncertainty values, and seven cases are analyzed in which the uncertainty level coefficient ξ of interval parameters are ±0.05, ±0.075, ±0.1, ±0.125, ±0.15, ±0.175, and ±0.2, respectively. Eight subintervals are implemented in the uncertainty space.

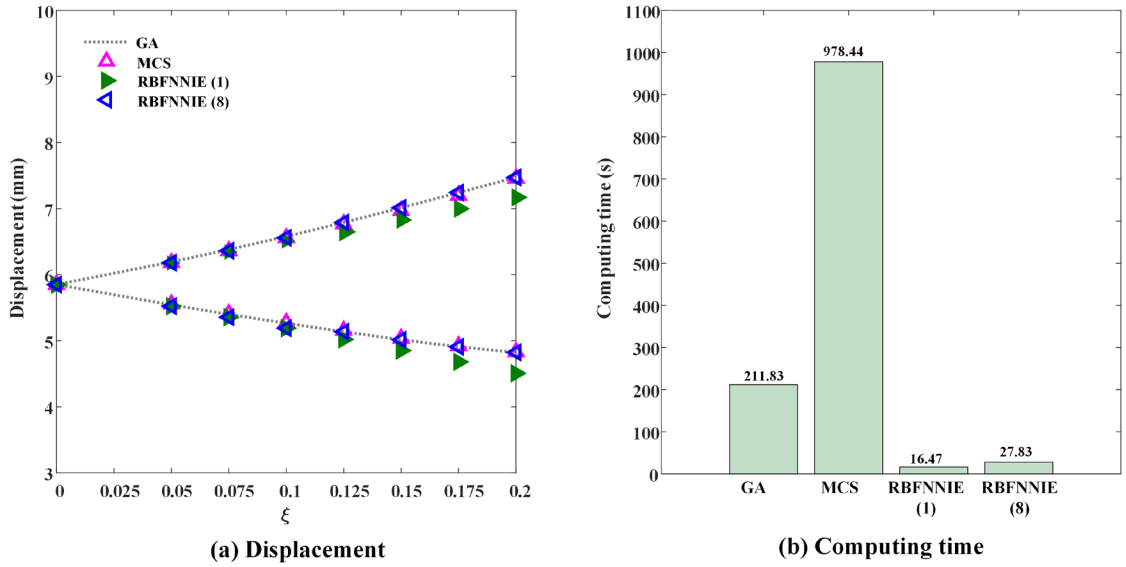

Fig. 9 Uncertainty analysis of displacement for arm.

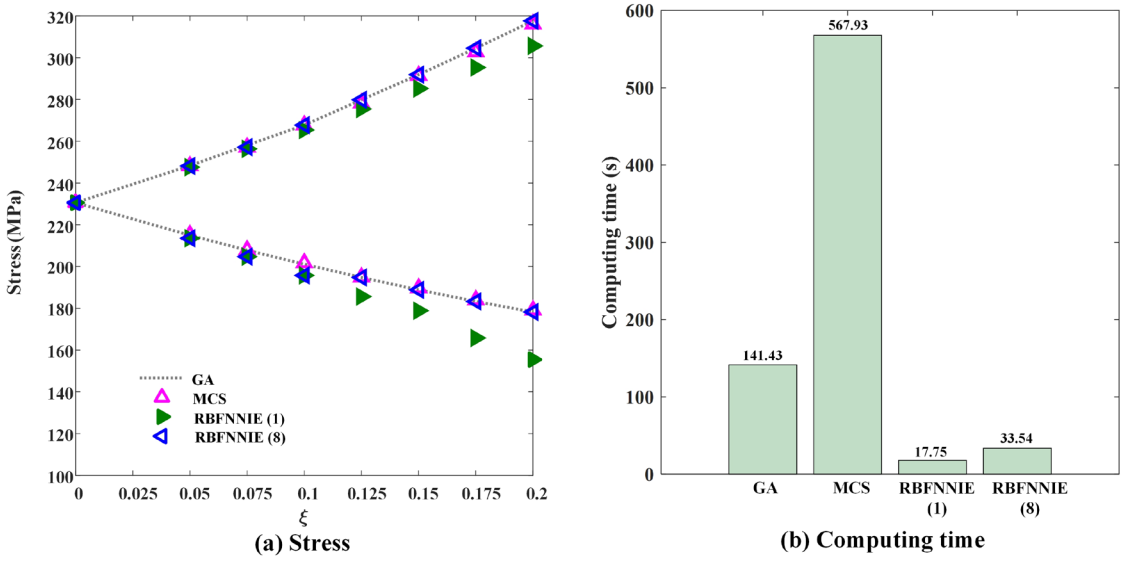

Fig. 10 Uncertainty analysis of von Mises stress for arm.

As shown in **Fig. 9** (a) and **Fig. 10** (a), the results of different uncertainty interval bounds are presented. Compared with GA, MCS and RBFNNIE (8) can effectively approximate the lower and

upper bounds of the displacement and stress. Because of the uncertainty deviation of design variables caused by machining problems, it will cause displacement and stress exceeding the expected value, and will bring the failure hazard of mechanical structures. As a random calculation method, MCS needs to consume more computing time. In **Fig. 9** (b), the average calculation time of MCS for displacement is 978.44s, while RBFNNIE (8) only needs 27.83s. In **Fig. 10** (b), the average calculation time of MCS for stress is 567.93s, while RBFNNIE (8) only needs 33.54s. It implies that RBFNNIE has higher efficiency. It is found that the error of RBFNNIE (1) increases obviously with the increase of uncertainty level, thus, RBFNNIE (1) is not suitable for interval analysis with the increase of uncertainty level. For the accuracy of lower and upper bounds of displacement and stress, the relative absolute errors of MCS and RBFNNIE relative to GA are given in **Table 3** and **Table 4**. The maximum error of MCS is 0.0353 in the upper bound with $\xi = 0.1$, and the maximum error of RBFNNIE (8) is 0.0197 appearing in the lower bound with $\xi = 0.2$. It shows that RBFNNIE (8) has a good approximation ability for the lower and upper bounds of the mechanical claw. The proposed method can be used to analyze the static loading problem.

Table 3 Relative absolute errors of displacement with different analysis methods

ξ	Lower bound			Upper bound		
	MCS	RBFNNIE (1)	RBFNNIE (8)	MCS	RBFNNIE (1)	RBFNNIE (8)
0.05	0.0023	0.0035	0.0017	0.0020	0.0026	0.0019
0.075	0.0018	0.0080	0.0019	0.0028	0.0058	0.0030
0.100	0.0021	0.0142	0.0056	0.0031	0.0103	0.0031
0.125	0.0038	0.0223	0.0057	0.0034	0.0162	0.0044
0.150	0.0039	0.0327	0.0093	0.0061	0.0233	0.0091
0.175	0.0028	0.0465	0.0169	0.0060	0.0308	0.0106
0.200	0.0016	0.0656	0.0170	0.0064	0.0372	0.0164

Table 4 Relative absolute errors of von Mises stress with different analysis methods

ξ	Lower bound			Upper bound		
	MCS	RBFNNIE (1)	RBFNNIE (8)	MCS	RBFNNIE (1)	RBFNNIE (8)
0.05	0.0013	0.0067	0.0018	0.0006	0.0030	0.0009
0.075	0.0008	0.0148	0.0011	0.0037	0.0067	0.0017
0.100	0.0034	0.0267	0.0018	0.0353	0.0157	0.0045
0.125	0.0008	0.0469	0.0125	0.0058	0.0262	0.0086
0.150	0.0046	0.0529	0.0149	0.0015	0.0327	0.0151
0.175	0.0040	0.0955	0.0157	0.0058	0.0703	0.0155
0.200	0.0050	0.1278	0.0197	0.0049	0.0847	0.0163

4.3 Anti-collision structures

Anti-collision structures can protect passengers by transforming external impact kinetic energy into plastic deformation energy. As shown in **Fig. 11**, the two crash models of the front-end anti-collision structures are carried out by the nonlinear explicit FE code LS-DYNA, the automatic single surface contact is applied to avoid penetration during deformation. The front-end anti-collision structure mainly includes three thickness parameters (T_1, T_2 and T_3 are 1mm). The material is steel and the mechanical properties are as follows: density $\rho = 7.83\text{g/cm}^3$; Young's modulus $E = 207\text{GPa}$; Poison's ratio $\nu = 0.28$, initial yield stress $\sigma_y = 346\text{MPa}$. A rigid wall is an impactor with an additional mass of 900 kg and an initial velocity of 50 km/h. The crushing deformations of the two models are presented in **Fig. 12**. Compared with frontal impact (crash angle is 0°), the anti-collision structure under oblique angle impact is prone to instability, the plastic deformation is irregular, and the energy absorption capacity will be reduced. Therefore, the anti-collision structure with superior crashworthiness performance should have a variety of oblique angle impact resistance. The main crashworthiness indicators include energy absorption and peak crushing force (*PCF*).

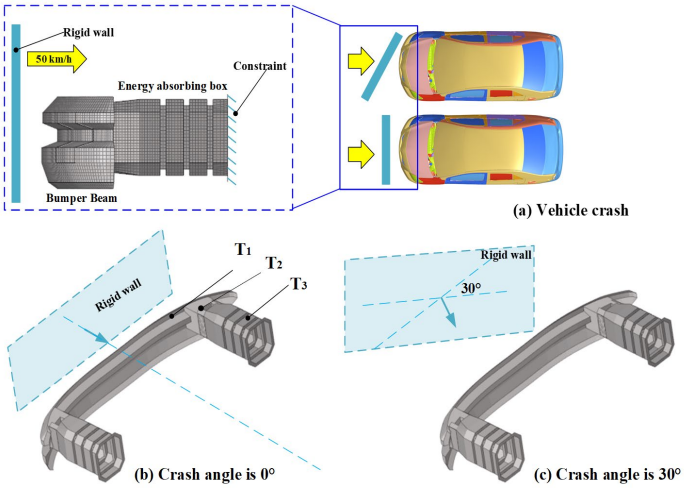

Fig. 11 Dynamic finite element model of anti-collision structures.

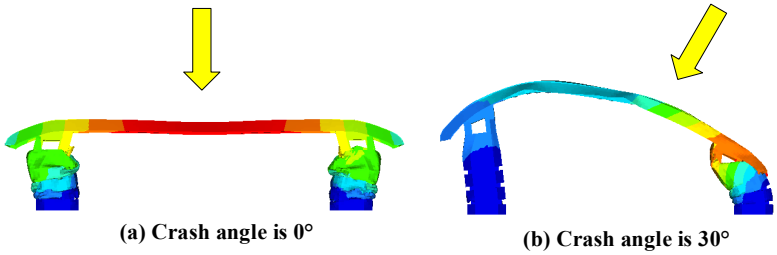

Fig. 12 Deformation behaviors of anti-collision structures

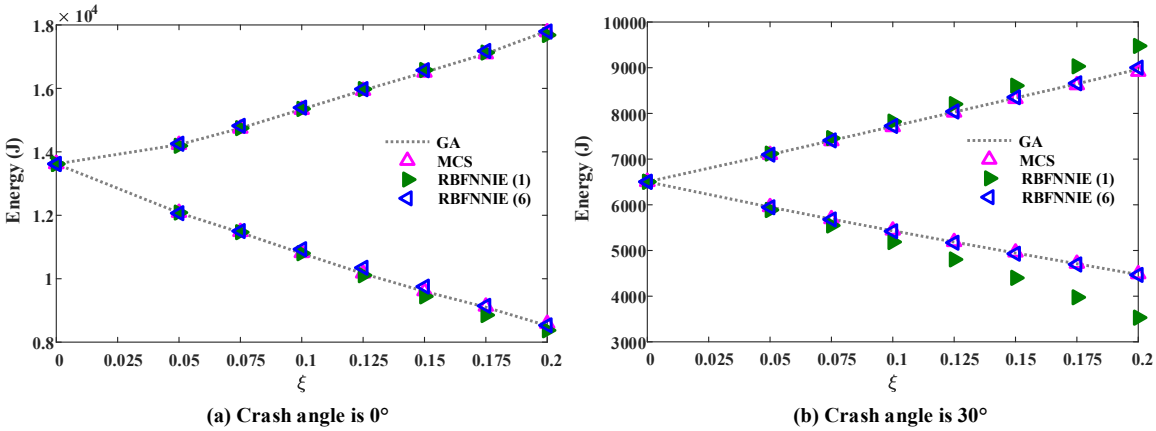

Fig. 13 Uncertainty analysis of energy absorption.

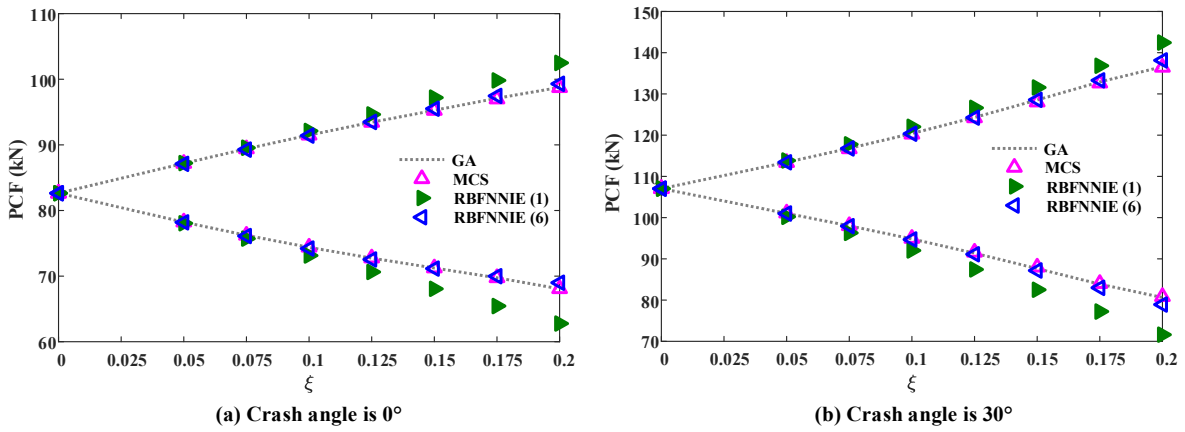

Fig. 14 Uncertainty analysis of peak crushing force.

To investigate the dynamic crushing characteristics of the anti-collision structure, three thickness parameters are regarded as interval uncertainty values, and seven cases are analyzed. Six subintervals are implemented in the uncertainty space. As shown in **Fig. 13** and **Fig. 14**, the results of different uncertainty interval bounds are presented. Compared with GA, MCS and RBFNNIE (4) can effectively approximate the lower and upper bounds of the displacement and stress responses. However, the errors of RBFNNIE (1) are still significant in all the indicators. For the accuracy of lower and upper bounds of the dynamic crushing models, the maximum relative errors of MCS and RBFNNIE relative to GA are given in **Table 5**. The maximum relative errors of MCS and RBFNNIE (6) are less than 0.03. It shows that MCS and RBFNNIE (6) have a good approximation ability for the lower and upper bounds of energy and *PCF*. As shown in **Fig. 15**, the maximum calculation time of MCS and RBFNNIE (6) is 1105.06s and 13.03s, respectively. The average calculation time of MCS is more than RBFNNIE (6). It should not be ignored that although GA and MCS can effectively find the boundary values of energy and *PCF*, their computational cost is expensive. Therefore, RBFNNIE can be used as an efficient and feasible scheme to solve the uncertain responses of dynamic crushing models.

Table 5 Maximum relative absolute errors of different analysis methods for the front anti-collision structure

NO.	Crash angle (°)	Responses	MCS	RBFNNIE (1)	RBFNNIE (6)
1	0	Energy	0.0077	0.0273	0.0181
2	0	PCF	0.0005	0.0778	0.0134
3	30	Energy	0.0058	0.2106	0.0097
4	30	PCF	0.0027	0.1117	0.0238

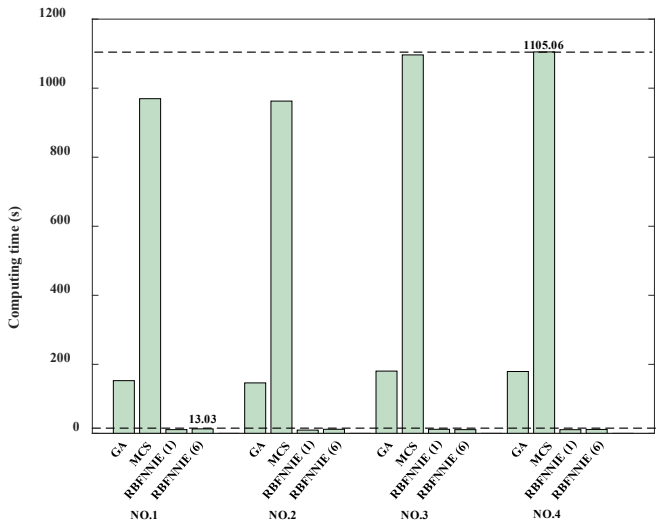

Fig. 15 Computing time for anti-collision structure.

4.4 Multi-link suspension

Multi-link suspension can not only ensure a certain degree of comfort but also make the wheels and the ground as vertical as possible and reduce the tilt of the body as much as possible. The kinematic model of multi-link suspension is established by ADMAS, and the travel of parallel wheel jump test is ±50mm, as shown in **Fig. 16**. Here, the toe angle, camber angle, wheel-track, and wheelbase are taken as the performance responses, and the main coordinate values with a prominent contribution of the four coordinates are obtained by significance analysis, as shown in **Table 6**. Four coordinate points are regarded as interval uncertainty parameters, and five cases are analyzed in which the uncertainty deviation, that is ±1mm, ±2mm, ±3mm, ±4mm, and ±5mm. Eight subintervals are implemented in the uncertainty space. The suspension with superior kinematic characteristics should keep the minimum change of toe angle, camber angle, wheel-track, and wheelbase in the wheel jump stroke. Therefore, the lower and upper bounds of the maximum and minimum values of different performance responses are considered. As shown in **Fig. 17**, the results of different uncertainty interval bounds are presented. It is easy to find that the uncertainty of the hardpoint is the most sensitive to toe angle by comparing the fluctuation range of different responses. Compared with GA, MCS and RBFNNIE (8) can effectively approximate the lower and upper bounds of the toe angle, camber angle, wheel-track, and wheelbase.

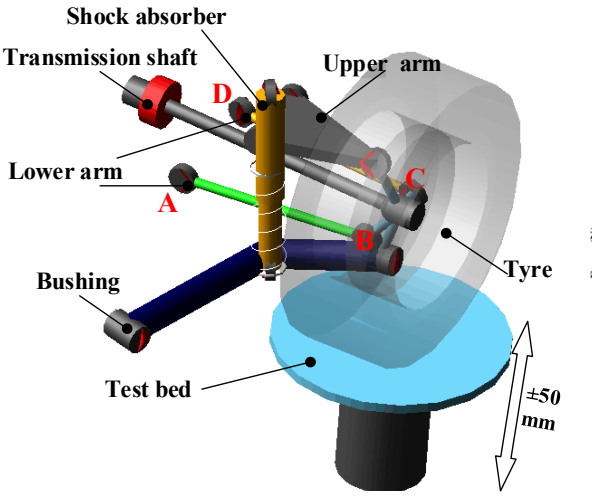

Fig. 16 Kinematic model of multi-link suspension.

For the accuracy of lower and upper bounds of the kinematic responses, the maximum errors of MCS and RBFNNIE relative to GA are given in **Table 7**. The maximum errors of MCS and RBFNNIE (8) are less than 0.02. It shows that RBFNNIE (8) has a good approximation ability for the lower and upper bounds of kinematic responses. The proposed method can obtain the feasible boundary solutions of multi-link suspension. In addition, the maximum calculation time of MCS and RBFNNIE (8) is 12550s and 132.03s, respectively. The average calculation time of RBFNNIE (8) is less than MCS. Similar to the conclusion of the above case, although both GA and MCS can approach the lower and upper bounds of uncertainty, the computational cost is expensive. Therefore, the proposed method can be used to analyze the uncertain bounds of the kinematic problem. Compared with the above three cases, the number of uncertain variables in this model has increased to 6, and the calculation cost has also increased. It shows that the total calculation cost is positively related to the number of uncertain variables.

Table 6 Coordinate points.

Coordinate points	A	B	C	D
Y (mm)	-265	-714	-698	-280
Z (mm)	969	1019	988	955

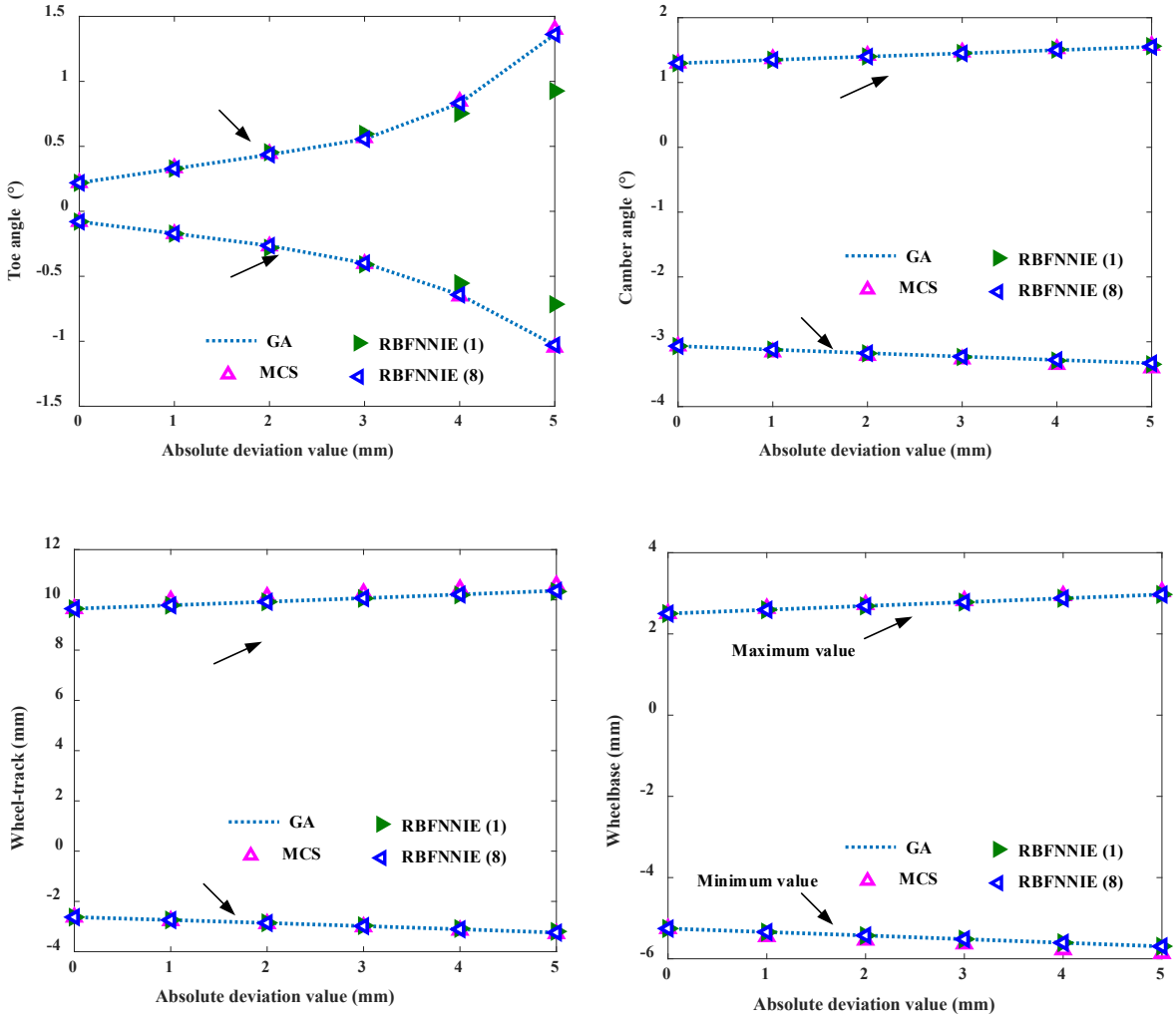

rack **(d) Wheelbase**

Fig. 17 Uncertainty analysis of multi-link suspension.

Table 7 Maximum relative absolute errors of different analysis methods.

NO.	Responses	MCS	RBFNNIE (1)	RBFNNIE (8)
1	Toe angle (Maximum)	0.0029	0.3195	0.0191
2	Toe angle (Minimum)	0.0075	0.1386	0.0105
3	Camber angle (Maximum)	0.0036	0.0070	0.0044
4	Camber angle (Minimum)	0.0021	0.0047	0.0029
5	Wheel-travel (Maximum)	0.0014	0.0030	0.0021
6	Wheel-travel (Minimum)	0.0028	0.0145	0.0058
7	Wheelbase (Maximum)	0.0003	0.0005	0.0002
8	Wheelbase (Minimum)	0.0002	0.0006	0.0002

5. Conclusion

To analyze the lower and upper bounds of interval uncertainty responses, a feasible identification method of uncertainty responses is proposed for vehicle structures with interval design parameters. The trained RBFNN parameters from the improved K-means clustering algorithm and singular value decomposition can approximate the first-order and second-order partial derivatives of different test functions. RBFNN provides a feasible way to calculate partial derivatives for Taylor expansion. During the analysis of engineering design models, GA, MCS, and RBFNNIE all can effectively and accurately approximate the lower and upper bounds of the uncertain structural responses. However, GA and MCS need more calculation time than RBFNNIE. RBFNNIE demonstrates higher feasibility and efficiency over the existing methods for uncertainty analysis. RBFNNIE with subintervals has higher accuracy than RBFNNIE (1) for all engineering design models. It is a feasible measure to increase the calculation accuracy by adding subintervals, while not increasing the computational cost.

The uncertainty of different engineering applications (vehicle hood, mechanical claw, anti-collision structures, and multi-link suspension) is analyzed, including vibration modal, static loading, nonlinear dynamic crushing, and kinematics problems. All the above results show that this proposed method has high applicability for vehicle design, and can carry out the optimization work of uncertain variables in the future.

Funding

This work was supported by the Prospective Technology Project of Nanchang Intelligent New Energy Vehicle Research Institute (17092380013), the Project of Shanghai Science and Technology Committee (20511104602), and the National Natural Science Foundation of China (52075188).

Ethics declarations

Conflict of interest

The authors declare that they have no conflict of interest.

Replication of results

The main program in this study can be found at https://github.com/xiangxu888/FOR_SHARING.git. More related data and codes that support the findings of this study are available from the first author or corresponding author upon reasonable request.

References

Almarashi AAS (2012) Approximation Solution of Fractional Partial Differential Equations by Neural Networks. Advances in Numerical Analysis 2012: 912810. https://doi.org/10.1155/2012/912810

Awad M, Qasrawi I (2018) Enhanced RBF neural network model for time series prediction of solar cells panel depending on climate conditions (temperature and irradiance). Neural Computing and Applications 30: 1757-1768. https://doi.org/10.1007/s00521-016-2779-5

Brown D, Ling L, Kansa E, Levesley J (2005) On approximate cardinal preconditioning methods for solving PDEs with radial basis functions. Engineering Analysis with Boundary Elements 29: 343-353. https://doi.org/10.1016/j.enganabound.2004.05.006

Cao L, Liu J, Xie L, Jiang C, Bi R (2021) Non-probabilistic polygonal convex set model for structural uncertainty quantification. Applied Mathematical Modelling 89: 504-518. https://doi.org/10.1016/j.apm.2020.07.025

Chen G, Yang D (2021) A unified analysis framework of static and dynamic structural reliabilities based on direct probability integral method. Mechanical Systems and Signal Processing 158: 107783. https://doi.org/10.1016/j.ymssp.2021.107783

Chen H, Kong L, Leng WJ (2011) Numerical solution of PDEs via integrated radial basis function networks with adaptive training algorithm. Applied Soft Computing 11: 855-860. https://doi.org/10.1016/j.asoc.2010.01.005

Chen SH, Ma L, Meng GW, Guo R (2009) An efficient method for evaluating the natural frequencies of structures with uncertain-but-bounded parameters. Computers & Structures 87: 582-590. https://doi.org/10.1016/j.compstruc.2009.02.009

Cheng J, Tang MY, Liu ZY, Tan JR (2016) Direct reliability-based design optimization of uncertain structures with interval parameters. Journal of Zhejiang University-SCIENCE A 17: 841-854. https://doi.org/10.1631/jzus.A1600143

Fernandez-Prieto JA, Canada-Bago J, Gadeo-Martos MA, Velasco JR (2012) Optimisation of control parameters for genetic algorithms to test computer networks under realistic traffic loads. Applied Soft Computing 12: 1875-1883. https://doi.org/10.1016/j.asoc.2011.02.004

Gao W, Wu D, Gao K, Chen X, Tin-Loi F (2018) Structural reliability analysis with imprecise random and interval fields. Applied Mathematical Modelling 55: 49-67. https://doi.org/10.1016/j.apm.2017.10.029

Gao W, Wu D, Song C, Tin-Loi F, Li X (2011) Hybrid probabilistic interval analysis of bar structures with uncertainty using a mixed perturbation Monte-Carlo method. Finite Elements in Analysis and Design, 47: 643-652. https://doi.org/10.1016/j.finel.2011.01.007

Guo X, Bai W, Zhang W (2008) Extreme structural response analysis of truss structures under material uncertainty via linear mixed 0–1 programming. International Journal for Numerical Methods in Engineering 76: 253-277. https://doi.org/10.1002/nme.2298

Huang ZL, Jiang C, Zhou YS, Luo Z, Zhang Z (2016) An incremental shifting vector approach for reliability-based design optimization. Structural and Multidisciplinary Optimization 53: 523-543. https://doi.org/10.1007/s00158-015-1352-7

Impollonia N, Muscolino G (2011) Interval analysis of structures with uncertain-but-bounded axial stiffness. Computer Methods in Applied Mechanics and Engineering 200: 1945-1962. https://doi.org/10.1016/j.cma.2010.07.019

Imani M, Ghoreishi SF (2021) Two-Stage Bayesian Optimization for Scalable Inference in State-Space Models. IEEE Transactions on Neural Networks and Learning Systems. https://doi.org/10.1109/TNNLS.2021.3069172

Jiang C, Han X, Liu GP (2008a) A sequential nonlinear interval number programming method for uncertain structures. Computer Methods in Applied Mechanics and Engineering 197: 4250-4265. https://doi.org/10.1016/j.cma.2008.04.027

Jiang C, Han X, Liu GR, Liu GP (2008b) A nonlinear interval number programming method for uncertain optimization problems. European Journal of Operational Research 188: 1-13. https://doi.org/10.1016/j.ejor.2007.03.031

Leonard JA, Kramer MA, Ungar LH (1992) Using radial basis functions to approximate a function and its error bounds. IEEE Transactions on Neural Networks 3: 624-627. https://doi.org/10.1109/72.143377

Li F, Luo Z, Rong J, Zhang N (2013) Interval multi-objective optimisation of structures using adaptive Kriging approximations. Computers & Structures 119: 68-84. https://doi.org/10.1016/j.compstruc.2012.12.028

Long XY, Mao DL, Jiang C, Wei FY, Li GJ (2019) Unified uncertainty analysis under probabilistic, evidence, fuzzy and interval uncertainties. Computer Methods in Applied Mechanics and Engineering 355: 1-26. https://doi.org/10.1016/j.cma.2019.05.041

Ma M, Wang L (2021) Reliability-based topology optimization framework of two-dimensional phononic crystal band-gap structures based on interval series expansion and mapping conversion method. International Journal of Mechanical Sciences 196: 106265. https://doi.org/10.1016/j.ijmecsci.2020.106265

Meng X, Liu J, Cao L, Yu Z, Yang D (2020) A general frame for uncertainty propagation under multimodally distributed random variables. Computer Methods in Applied Mechanics and Engineering 367: 113109. https://doi.org/10.1016/j.cma.2020.113109

Qiu Z, Chen S, Elishakoff I (1996) Bounds of eigenvalues for structures with an interval description of uncertain-but-non-random parameters. Chaos, Solitons & Fractals 7: 425-434. https://doi.org/10.1016/0960-0779(95)00065-8

Qiu Z, Li X (2021) A new model for the eigenvalue buckling analysis with unknown-but-bounded parameters. Aerospace Science and Technology 113: 106634. https://doi.org/10.1016/j.ast.2021.106634

Qiu Z, Ma L, Wang X (2009) Non-probabilistic interval analysis method for dynamic response analysis of nonlinear systems with uncertainty. Journal of Sound and Vibration 319: 531-540. https://doi.org/10.1016/j.jsv.2008.06.006

Qiu Z, Wang X (2005a) Parameter perturbation method for dynamic responses of structures with uncertain-but-bounded parameters based on interval analysis. International Journal of Solids and Structures 42: 4958-4970. https://doi.org/10.1016/j.ijsolstr.2005.02.023

Qiu Z, Wang X (2005b) Solution theorems for the standard eigenvalue problem of structures with uncertain-but-bounded parameters. Journal of Sound and Vibration 282: 381-399. https://doi.org/10.1016/j.jsv.2004.02.024

Qiu Z, Wang X, Chen J (2006) Exact bounds for the static response set of structures with uncertain-but-bounded parameters. International Journal of Solids and Structures 43: 6574-6593. https://doi.org/10.1016/j.ijsolstr.2006.01.012

Qiu Z, Xia Y, Yang J (2007) The static displacement and the stress analysis of structures with bounded uncertainties using the vertex solution theorem. Computer Methods in Applied Mechanics and Engineering 196: 4965-4984. https://doi.org/10.1016/j.cma.2007.06.022

Rageh A, Eftekhar AS, Linzell DG (2020) Steel railway bridge fatigue damage detection using numerical models and machine learning: Mitigating influence of modeling uncertainty. International Journal of Fatigue 134:105458. https://doi.org/10.1016/j.ijfatigue.2019.105458

Sharifzadeh M, Sikinioti-Lock A, Shah N (2019) Machine-learning methods for integrated renewable power generation: A comparative study of artificial neural networks, support vector regression, and Gaussian Process Regression. Renewable and Sustainable Energy Reviews 108: 513-538. https://doi.org/10.1016/j.rser.2019.03.040

Toyota Yaris (2016) finite element model. https://www.ccsa.gmu.edu/models/2010-toyota-yaris/. Released December 2016.

Tang T, Luo H, Song Y, Fang H, Zhang J (2021) Chebyshev inclusion function based interval kinetostatic modeling and parameter sensitivity analysis for Exechon-like parallel kinematic machines with parameter uncertainties. Mechanism and Machine Theory 157: 104209. https://doi.org/10.1016/j.mechmachtheory.2020.104209

Viegas C, Daney D, Tavakoli M, De Almeida AT (2017) Performance analysis and design of parallel kinematic machines using interval analysis. Mechanism and Machine Theory 115: 218-236. https://doi.org/10.1016/j.mechmachtheory.2017.05.003

Wang L, Chen Z, Yang G, Sun Q, Ge J (2020). An interval uncertain optimization method using back-propagation neural network differentiation. Computer Methods in Applied Mechanics and Engineering 366: 113065.

https://doi.org/10.1016/j.cma.2020.113065

Warnes MR, Glassey J, Montague GA, Kara B (1998) Application of radial basis function and feedforward artificial neural networks to the Escherichia coli fermentation process. Neurocomputing 20: 67-82. https://doi.org/10.1016/S0925-2312(98)00025-3

Wu J, Zhao You Q, Chen Su H (2005) An improved interval analysis method for uncertain structures. Structural Engineering and Mechanics 20: 713-726. https://doi.org/10.12989/sem.2005.20.6.713

Wu J, Luo Z, Zhang Y, Zhang N (2014) An interval uncertain optimization method for vehicle suspensions using Chebyshev metamodels. Applied Mathematical Modelling 38: 3706-3723. https://doi.org/10.1016/j.apm.2014.02.012

Xia B, Lü H, Yu D, Jiang C (2015) Reliability-based design optimization of structural systems under hybrid probabilistic and interval model. Computers & Structures 160: 126-134. https://doi.org/10.1016/j.compstruc.2015.08.009

Xu X, Chen X, Liu Z, Xu Y, Zhang Y (2021a) Reliability-based design for lightweight vehicle structures with uncertain manufacturing accuracy. Applied Mathematical Modelling 95: 22-37. https://doi.org/10.1016/j.apm.2021.01.047

Xu X, Chen X, Liu Z, Yang J, Xu Y, Zhang Y, Gao Y (2021b) Multi-objective reliability-based design optimization for the reducer housing of electric vehicles. Engineering Optimization . https://doi.org/10.1080/0305215X.2021.1923704

Zhang D, Zhang N, Ye N, Fang J, Han X (2020) Hybrid Learning Algorithm of Radial Basis Function Networks for Reliability Analysis. IEEE Transactions on Reliability. https://doi.org/10.1109/TR.2020.3001232

Zhang XM, Ding H, Chen SH (2007) Interval finite element method for dynamic response of closed-loop system with uncertain parameters. International Journal for Numerical Methods in Engineering 70: 543-562. https://doi.org/10.1002/nme.1891